# Compartmentalizing a lipid bilayer by tuning lateral stress in a physisorbed polymer-tethered membrane†

**Amanda P. Siegel,[a] Michael J. Murcia,[a] Merrell Johnson,[b] Michael Reif,[c] Rainer Jordan,‡[c] Jürgen Rühe[d] and Christoph A. Naumann*[a]**

***Received 21st January 2010, Accepted 15th April 2010***
***First published as an Advance Article on the web 7th May 2010***
**DOI: 10.1039/c001394c**

The current study reports the compartmentalization of a physisorbed polymer-tethered phospholipid bilayer built using subsequent Langmuir–Blodgett (LB) and Langmuir–Schaefer (LS) transfers, where compartmentalization is due to buckling in the bottom (LB) monolayer and polymer-specific stress relaxation processes. Buckling arises from lateral stress within the membrane induced by a high (15–30 mol%) concentration of poly(2-ethyl-2-oxazoline) lipopolymers in the LB monolayer. Epifluorescence microscopy (EPI) and fluorescence recovery after photobleaching (FRAP) experiments confirm the formation of a homogeneous bilayer at low lipopolymer molar concentrations (low lateral stress), but demonstrate the compartmentalization of the bilayer into μm size compartments at elevated lipopolymer concentrations (high lateral stress). Quantitative EPI of the LB monolayer as well as additional atomic force microscopy (AFM) experiments show that bilayer compartmentalization, buckling and partial delamination of the LB monolayer occur without causing notable phospholipid–lipopolymer phase separations, but do preclude bilayer formation above buckled/delaminated regions after LS transfer. As long-time tracking experiments of photostable quantum dot-conjugated lipids in the compartmentalized bilayer system confirm, our membrane system enables the facile adjustment of the permeability of diffusion boundaries between bilayer compartments, thus providing an excellent experimental tool to mimic length-scale dependent diffusion processes observed in cellular membranes. We expect that the fundamental concept of lateral stress regulation and buckling-associated membrane compartmentalization can also be applied to other polymer–lipid composite materials than the one studied in this work.

## Introduction

The response of ultrathin elastic sheets to lateral stress represents a fascinating topic of study in a great variety of research areas as diverse as road construction,[1] microchip technology,[2] and pulmonary function.[3] Generally speaking, there are common failure mechanisms (or adaptive responses) which occur in all of these different systems, and for compression stresses, they fall into the following two categories: initially, buckling or wrinkling of the thin sheet; and finally, out of plane folding or collapse. When the material being compressed is a monolayer over a soft substrate such as an aqueous subphase, the buckling stage is represented by an isotropic wrinkling, and the collapse can result in formation of larger length-scale folds and a smoothing out of the wrinkles.[4] Interestingly, materials as diverse as thin polyester films and colloidal gold nanoparticles can reversibly generate wrinkles and, furthermore, folds, in reproducible patterns where the length scale of the fold is set by the wavelength of the wrinkle.[4,5] Along with wrinkling and folding, when the elastic film lies on a stiff substrate, delamination can also occur and this too has been exploited for patterning purposes.[2,6,7]

A fascinating example of ultrathin elastic sheet compression and expansion in nature is the human lung. Mammalian lung surfactant is comprised of a complex of phospholipids and lung proteins which form a monolayer covering the lung surface. This monolayer, which helps reduce the surface tension of the lungs during breathing, undergoes a reversible "collapse", or out of plane folding, during normal breathing cycles.[8] Significantly, there is no phase separation during this wrinkling and folding. Model monolayers representing human lungs have been studied, but pure lipid mixtures undergo an initial wrinkling and then irreversibly fold and collapse unless surfactant lung proteins, specifically SP-B or SP-C comprising about 10% of the mixture, are included in the model system.[9] Surfactant lung proteins also prevent phase separations among the lipids during compression. Molecular dynamic simulations on pure lipid and lipid–protein studies have confirmed these fascinating findings.[10,11]

Here, we show for the first time that stress-induced buckling patterns can also be formed in lipopolymer-containing lipid

[a]*Department of Chemistry and Chemical Biology, Indiana University-Purdue University Indianapolis, Indianapolis, IN, 46202-3274, USA. E-mail: canauman@iupui.edu*
[b]*Department of Physics, Indiana University-Purdue University Indianapolis, Indianapolis, IN, 46202-3274, USA*
[c]*Technical University of Munich, Department of Macromolecular Chemistry, 85747 Garching bei München, Germany*
[d]*University of Freiburg—IMTEK Department of Microsystems Engineering, Laboratory for Chemistry and Physics of Interfaces, 79110 Freiburg, Germany*

† Electronic supplementary information (ESI) available: Additional EPI images of compartmentalized bilayers. See DOI: 10.1039/c001394c

‡ Current address: Technical University of Dresden, Department of Chemistry, 01062 Dresden, Germany.

membrane systems by adjusting the molar concentration of cone-shaped lipopolymers consisting of a lipid anchor covalently linked to a relatively bulky hydrophilic polymer moiety. Previously, such polymer-tethered membrane systems on solids[12,13] have been employed to investigate, for example, the lateral mobility and functionality of reconstituted membrane proteins[14–20] and the transbilayer coupling of raft-mimicking domains[21,22] and to specifically tailor the construct morphology.[23] Traditionally, these experiments are conducted using low molar concentrations of lipopolymers in the bottom leaflet of the bilayer. Earlier wide-field single molecule fluorescence microscopy (SMFM) experiments on physisorbed polymer-tethered membranes of various lipopolymer concentrations by our group, which probed a length scale of up to 100 nm, also demonstrated that the presence of lipopolymers is associated with intriguing properties of membrane dynamics, including obstacle-induced obstructed diffusion of lipids and membrane proteins and transbilayer coupling of obstructed diffusion.[14,24] These effects are distinct from those obtained using corresponding membrane systems characterized by chemisorbed lipopolymers.[17] In the current work, we show that lipopolymer-induced bilayer stress regulation in a physisorbed system also has a profound influence on the membrane organization and dynamics at larger length scales. Initially, stable buckling patterns are created in polymer-tethered lipid monolayers built using Langmuir–Blodgett (LB) monolayer transfer without inducing notable lipopolymer–lipid demixing. Remarkably, epifluorescence microscopy (EPI) and atomic force microscopy (AFM) experiments on polymer-tethered lipid bilayers show that lipid bilayer formation after subsequent Schaefer (LS) transfer is inhibited at buckling regions when the polymer moiety of the lipopolymer system is moderately lipophilic. Fluorescence recovery after photobleaching (FRAP) and long-term single molecule tracking of quantum dot (QD)-conjugated lipids show that "bilayer-dewetted" buckling regions become lipid diffusion barriers, and the bilayer permeability can be tuned *via* the lipopolymer molar concentration. Notably, the current bilayer-compartmentalization method presents an attractive alternative to existing approaches for compartmentalizing or patterning model membrane systems using mostly microfabrication methods[25–30] because it is entirely based on the controlled regulation of lateral stress *via* changes in membrane composition in the presence of cone-shaped molecules (lipopolymers). While microfabrication-based methods result in more well-defined bilayer patterns, the current approach is of interest as a superior mimetic of bilayer compartmentalization in plasma membranes caused by the underlying cytoskeleton.[31] Akin to conditions in cellular membranes, bilayer compartments in physisorbed polymer-tethered bilayer systems show significant confinement, but also enable membrane molecules to cross compartment barriers. In addition, the ability to regulate the bilayer fluidity in these membrane systems at various length scales[14,24] not only provides a fascinating tool to study diffusion-controlled processes in biological membranes under well-defined conditions, but also may be useful for technological applications as well.

## Experimental

### Materials

The lipopolymer dioctadecylamine poly(2-ethyl-2-oxazoline)$_{85}$ (DODA-E$_{85}$) was synthesized following a procedure described previously.[32] The lipopolymers 1,2-dioctadecyl-*sn*-glycero-3-*N*-poly(2-methyl-2-oxazoline)$_{50}$ (diC$_{18}$M$_{50}$), 1,2-dioctadecyl-*sn*-glycero-3-*N*-poly(2-ethyl-2-oxazoline)$_{50}$ (diC$_{18}$E$_{50}$), and 1,2-dioctadecyl-*sn*-glycero-3-*N*-poly(2-ethyl-2-oxazoline)$_{50}$ with a terminal fluorescence label of 6-tetramethylrhodamine-thiocarbamoyl (diC$_{18}$E$_{50}$-TRITC) were synthesized following procedures described previously.[33,34] DODA-E$_{85}$, diC$_{18}$E$_{50}$, diC$_{18}$E$_{50}$-TRITC and diC$_{18}$M$_{50}$ are shown in Fig. 1. The phospholipids 1-stearoyl-2-oleoyl-*sn*-glycero-3-phosphocholine (SOPC), 1,2-dipalmitoyl-*sn*-glycero-3-phosphocholine (DPPC) and 1,2-dipalmitoyl-*sn*-glycero-3-phosphothioethanol (DPTE), and the PEG lipopolymers 1,2-distearoyl-*sn*-glycero-3-phosphoethanol amine-*n*-[methoxy(polyethylene glycol)-2000] (DSPE-PEG2000), and 1,2-distearoyl-*sn*-glycero-3-phosphoethanolamine-*n*-[maleimide (polyethylene glycol)-2000] (DSPE-PEG2000-maleimide) were purchased from Avanti Polar Lipids (Alabaster, AL). The fluorescently labeled phospholipids *N*-(6-tetramethylrhodamine-thiocarbamoyl)-1,2-dihexadecanoyl-*sn*-glycero-3-phosphoethanolamine, triethylammonium salt (TRITC-DHPE) and *N*-(7-nitrobenz-2-oxa-1,3-diazol-4-yl)-1,2-dihexadec-anoyl-*sn*-glycero-3-phosphoethanolamine, triethylammonium salt (NBD-DHPE) were obtained from Invitrogen/Molecular Probes (Eugene, OR). Chloroform (HPLC grade, Fisher Scientific, Pittsburgh, PA) was used as a spreading solvent for preparing SOPC and SOPC/lipopolymer monolayers at the air–water interface and Milli-Q water (pH = 5.5, 18 MΩ cm

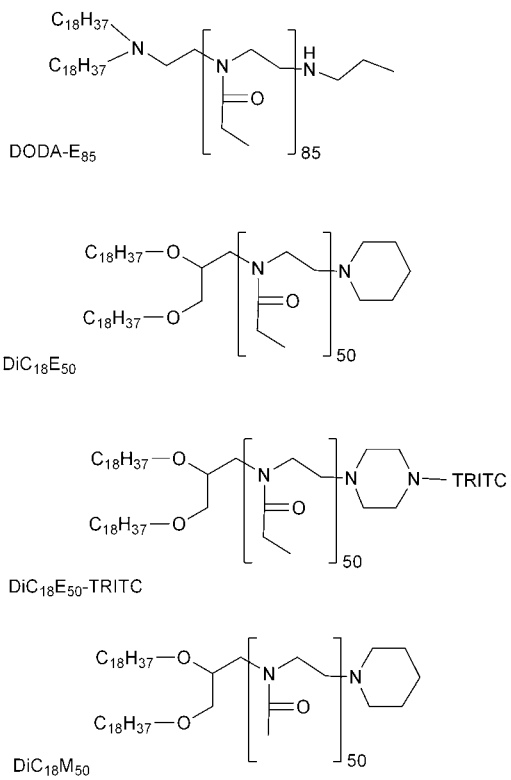


**Fig. 1** Chemical structures of the lipopolymers: dioctadecylamine poly(2-ethyl-2-oxazoline)$_{85}$ (DODA-E$_{85}$), 1,2-dioctadecyl-*sn*-glycero-3-*N*-poly(2-ethyl-2-oxazoline)$_{50}$ (diC$_{18}$E$_{50}$), 1,2-dioctadecyl-*sn*-glycero-3-*N*-poly(2-ethyl-2-oxazoline)$_{50}$-TRITC (diC$_{18}$E$_{50}$-TRITC) and 1,2-dioctadecyl-*sn*-glycero-3-*N*-poly(2-methyl-2-oxazoline)$_{50}$ (diC$_{18}$M$_{50}$).

resistivity; Milli-Q, Millipore, Billerica, MA) was used as a subphase material for all experiments. For the formation of QDs, cadmium acetate and elemental selenium pellets were purchased from Strem Chemicals (Newburyport, MA). Trioctylphosphine, trioctylphosphine oxide, tributylphosphine, hexadecylamine, zinc nitrate hexahydrate, potassium ethylxanthate and HPLC grade solvents were purchased from Aldrich Chemical (Milwaukee, WI).

### Formation of QD-conjugated lipids

CdSe/ZnS core/shell QDs were synthesized using a sonochemical approach reported previously.[35] In short, cadmium acetate and selenium dissolved in trioctylphosphine were sonicated in a coordinating bath of trioctylphosphine oxide and hexadecylamine until their fluorescent properties displayed a peak around 540 nm, and then were shelled by sonication of the dots with zinc ethyl xanthate dissolved in tributylphosphine which increased their peak emission to around 570 nm. Lipopolymer encapsulation was carried out following the procedure recently published.[36] In brief, the dots were removed from their coordinating solvent and coated with a mixture of DSPE-PEG2000, DSPE-PEG2000-maleimide, and DPPC in a 39 : 1 : 60 mole ratio, and suspended in water. Subsequently, the QDs were added to the aqueous phase above a lipid bilayer containing a small concentration of DPTE and in about one hour, the QDs fused with DPTE lipids to form QD-conjugated lipids, as reported.[37]

### Construction of polymer-tethered phospholipid bilayer

Polymer-tethered phospholipid bilayers were built using successive LB and LS film transfers following standard procedures described before.[14,21,38] To form the first (LB) monolayer, a chloroform solution of a mixture of lipopolymers (DODA-$E_{85}$, di$C_{18}E_{50}$, di$C_{18}M_{50}$, or di$C_{18}E_{50}$) and phospholipids (SOPC), with either 1.0 mol% NBD-PE or 0.4–0.8 mol% TRITC-DHPE or di$C_{18}E_{50}$-TRITC for epifluorescent studies, was spread at the air–water interface of a film balance with dipper (Labcon, Darlington, UK). Next the monolayer was compressed and, after stabilization, transferred to a glass substrate at a film pressure of 30 mN $m^{-1}$, which corresponds to an average area per lipid of $A_{lipid} = 65$ Å$^2$ and a transfer rate of about 300 μm $s^{-1}$. To add the second (LS) monolayer, a chloroform solution containing SOPC was spread at the air–water interface and also compressed to a film pressure of 30 mN $m^{-1}$. To allow wide-field single molecule fluorescence microscopy (SMFM) and EPI experiments, this monolayer also contained either $10^{-8}$ mol% DPTE (SMFM) or 0.4–1 mol% dyed lipids (NBD-PE, TRITC-DHPE). LS transfer to complete the bilayer was accomplished by stabilizing the LS monolayer with a concave slide positioned underneath the air–water interface and then gently but forcefully pushing the glass substrate containing the LB layer onto the underlying concave slide. After removing the remaining lipids from the surface, this concave slide and glass substrate together could be imaged by EPI within 4 h or for SMFM studies with QD-conjugated lipids, the bilayer-containing glass substrate was assembled as the bottom part of a cuvette with a glass cylinder perched atop, and QD conjugation was achieved by adding maleimide-functionalized QDs to the cuvette and by rinsing off the excess (unbound) QDs as described recently.[37] Regulation of lateral stress in the polymer-tethered phospholipid bilayer is achieved by adjusting the molar concentration of cone-shaped lipopolymers, which consist of a small lipid anchor and a bulky polymer moiety. At 5 mol% lipopolymers (low lateral stress), polymer moieties have the ability to form a coil-like conformation of maximum entropy reflecting weak repulsive inter-polymer interactions. In contrast, at 15 mol% and even more at 30 mol% lipopolymers (enhanced lateral stress), increases in lipopolymer concentrations cause enhanced stretching and confinement of polymer moieties of lipopolymers, as well as increased repulsive inter-polymer interactions.

### Quantitative analysis of EPI micrographs

As described before,[21] EPI was conducted using an inverted optical microscope in epiillumination (Axiovert 200M, Zeiss, Oberkochen, Germany) where the beam was focused on the sample by a microscopy objective (Zeiss C-Apochromat, water immersion, 40× NA = 1.2 or Zeiss α plan-FLUAR TIRF, oil immersion, 100× NA = 1.45). EPI studies analyzing relative concentrations of lipids and lipopolymers through intensity analysis were undertaken utilizing a Zeiss AxioCam MRm monochrome digital camera and Axiovision 4.8 software. The exposure time for each micrograph was 50 ms. This generated consistent micrographs with a range of grey values, where the grey value (ranging from 32 for background to 3600 for monolayers with 0.8 mol% TRITC-DHPE) corresponded to the relative quantity of TRITC-DHPE or di$C_{18}E_{50}$-TRITC in different regions in the micrographs. The micrographs contained two distinct regions, "bright phase" and "dark phase" regions, and grey values were found for a representative sample of regions and micrographs for three different dye concentrations. A monolayer with no dye was also imaged to obtain appropriate background values. To compare the relative grey values between the two sets of data, the mean grey value for the bright region of the 0.8 mol% TRITC-DHPE monolayer and the bright region of 0.8 mol% di$C_{18}E_{50}$-TRITC monolayer was each assigned the value of 1000 a.u. (arbitrary units) and the rest of the grey values for that series, the TRITC-DHPE series or the di$C_{18}E_{50}$-TRITC series, were calculated relative to that number, in a.u.

For determination of compartment sizes of the 30 mol% DODA-$E_{85}$ bilayers through EPI microscopy, images were acquired and analyzed using a CoolSNAP$_{fx}$ charge-coupled device camera (Roper Scientific, Princeton, NJ) and Roper Scientific imaging software. Fluorescence recovery after photobleaching (FRAP) was performed by closing the field stop on the microscope to its smallest position and permitting the Hg light source (AttoArc HBO 100 Watt) to bleach the sample for 30 s. Two minutes or more passed before a subsequent EPI image was taken to show recovery. Determination of the size distribution of the compartments was performed using image analysis (Axiovision software). Here we determined a statistically significant number of compartment areas from different regions of the membrane. The average, $A_{EPI}$, and standard deviation were then determined for the set of analyzed compartments. The procedure was repeated on different samples to ensure reproducibility of the average compartment size. It is also possible to determine

average compartment size in a completely independent fashion, utilizing SMFM of photostable quantum dot-conjugated lipids as described below.

### Single molecule fluorescence microscopy (SMFM): analysis of bilayer compartment size

SMFM experiments on polymer-tethered bilayers were conducted as described recently.[14,24,37] In short, a 100 mW frequency doubled Nd:YAG laser (532 nm) was used as the excitation source, whose intensity was regulated by a continuously variable neutral density filter. The excitation beam was delivered to the EPI port of an inverted microscope (Zeiss Axiovert S100TV) equipped with the dichroic mirror DM (Omega XF1051), a Raman edge filter (Omega XR3002 540AELP) and focused by a high aperture objective (Zeiss Plan Neofluar, oil immersion, 100 × NA = 1.3 or Olympus UApo/340, water immersion, 40 × NA = 1.15). The fluorescent light was detected by an intensified CCD camera (iPentaMAX 512EFT, Princeton Instruments). A Uniblitz shutter (VMM-D1) of 3 mm open aperture was used to control the exposure time and lag time between images, and was synchronized with the electronic shutter within the CCD camera. The exposure time and the time lag between exposures were set to 10 and 38 ms, respectively. Shutter control, image acquisition and image analysis were performed with ISee Imaging software (ISee Imaging) installed on a Dell PC running the Fedora core 4 Linux platform. Tracking data were analyzed in terms of mean-square-displacement $\langle r^2 \rangle$ *versus* time, $\tau$, plots, where due to the high photostability of the QD probes, we were able to probe μm length scales. Here, $\langle r^2 \rangle$ *vs.* $\tau$ plots were obtained by determining the $x$, $y$ coordinates of individual probe molecules as a function of time and by averaging 150 tracks each from 150 separate probe molecules. As reported previously, this procedure assured a statistical error of $\langle r^2 \rangle$ at each determined time lag of <5%.[14] Analysis of the distribution of $r^2$ values at a fixed time lag showed that the immobile fraction of tracks for 5, 15, and 30 mol% lipopolymers does not exceed 2%, which is in good agreement with previous tracking results using dye-labeled lipids in the same experimental system.[14] Information about compartmentalization can be obtained from these plots because Brownian diffusion inside and between compartments is characterized by different diffusion coefficients, $D_{\text{micro}}$ and $D_{\text{macro}}$, and a characteristic time, $\tau_{\text{residency}}$, associated with the transition from $D_{\text{micro}}$ to $D_{\text{macro}}$. As described previously,[31] for roughly rectangular compartment geometries the average compartment size, $A_{\text{SMFM}}$, can be found directly from the relationship between $D_{\text{macro}}$ and $\tau_{\text{residency}}$. In the case of circular compartments, as observed in this study, residency time is related to compartment size as follows:

$$A_{\text{SMFM}} = \tau_{\text{residency}}/\pi D_{\text{macro}}. \quad (1)$$

### Atomic force microscopy

AFM images were obtained using a Digital Instruments BioScope, and analyzed using Nanoscope IV (Digital Instruments/Veeco Metrology Group, Plainview, NY). The samples were scanned using stiff ($k$ = 0.32 or 0.58 N m$^{-1}$) non-conductive silicon nitride cantilevers (Veeco Instruments). Usually, regions ranging from 5 × 5 μm$^2$ to 1 × 1 μm$^2$ were imaged at resolutions of 512 × 512 or 256 × 256 pixels using a scan rate of 1 Hz. Monolayers were analyzed in air within 24 hours of preparation using the tapping mode. Bilayers were analyzed under water in tapping mode within 24 hours of preparation by mounting the cantilever onto a water-tight cantilever-mount. Manual tuning was necessary for the underwater images and for fine-tuning the air images. Both height and phase data were taken.

## Results and discussion

We first conducted a set of EPI and FRAP experiments to explore the impact of applied lateral stress on the large-scale membrane organization and dynamics of a physisorbed polymer-tethered phospholipid bilayer. Fig. 2a–f illustrate representative EPI and FRAP micrographs of physisorbed polymer-tethered SOPC bilayers containing 5 (a and d), 15 (b and e), and 30 mol% (c and f) of the poly(2-ethyl-2oxazoline) lipopolymer DODA-$E_{85}$. While the top (LS) monolayer exclusively contains the phospholipid SOPC and 1 mol% dye-labeled lipid NBD-DHPE, the bottom (LB) monolayer is comprised of mixtures of NBD-DHPE, SOPC and DODA-$E_{85}$. At the low lipopolymer molar concentration of 5 mol%, the fluorescence micrograph shows a homogeneous bilayer (Fig. 2a). In this case, an isotropic fluorescence recovery can be observed (Fig. 2d), which resembles that of a one-component lipid bilayer in the fluid phase. In contrast, at 15 mol% DODA-$E_{85}$, the fluorescence micrograph suggests the existence of two distinct phases (Fig. 2b). Interestingly, the corresponding FRAP experiment shows that the darker phase acts as a lipid diffusion barrier, thus effectively compartmentalizing the bilayer system (Fig. 2e). At 30 mol% DODA-$E_{85}$, the dark phase becomes more pronounced and the bilayer compartmentalization becomes more complete (Fig. 2c and f). Comparable results were obtained when NBD-DHPE was replaced by TRITC-DHPE, thus excluding dye-specific artifacts as a possible explanation of the data in Fig. 2. Representative micrographs for 15 mol% DODA-$E_{85}$ with TRITC-DHPE instead of NBD-DHPE are provided in Fig. S1 of ESI†.

One possible explanation for the different phases in Fig. 2b, c, e and f is the formation of a large-scale phase separation into lipopolymer-poor and lipopolymer-rich (NBD-DHPE deficient) phases in the bottom leaflet (LB monolayer). In fact, recently it was reported that polymeric systems are able to corral lipids in a monolayer, thereby causing its compartmentalization.[39] In addition, lipopolymer–phospholipid phase separations have been reported on polymer-tethered lipid bilayer systems built using very slow LB transfer speeds.[40] To explore whether such phase separations would explain the micrographs shown in Fig. 2, LB monolayers of 15 mol% di$C_{18}E_{50}$ and 85 mol% SOPC were constructed with 0.4, 0.6, and 0.8 mol% dyed lipids (TRITC-DHPE) or 0.4, 0.6, and 0.8 mol% dyed lipopolymers (di$C_{18}E_{50}$-TRITC) quantitatively, as described above.§ Fig. 3 illustrates representative EPI micrographs of LB monolayers showing the dyed-lipid (top) and di$C_{18}E_{50}$-TRITC distributions (bottom) (dye-molecule concentration: 0.6 mol%).

§ The lipopolymer di$C_{18}E_{50}$ was utilized here because of the availability of the appropriate fluorescently labeled analogue and because di$C_{18}E_{50}$ contains the same polymeric moiety as DODA-$E_{85}$.

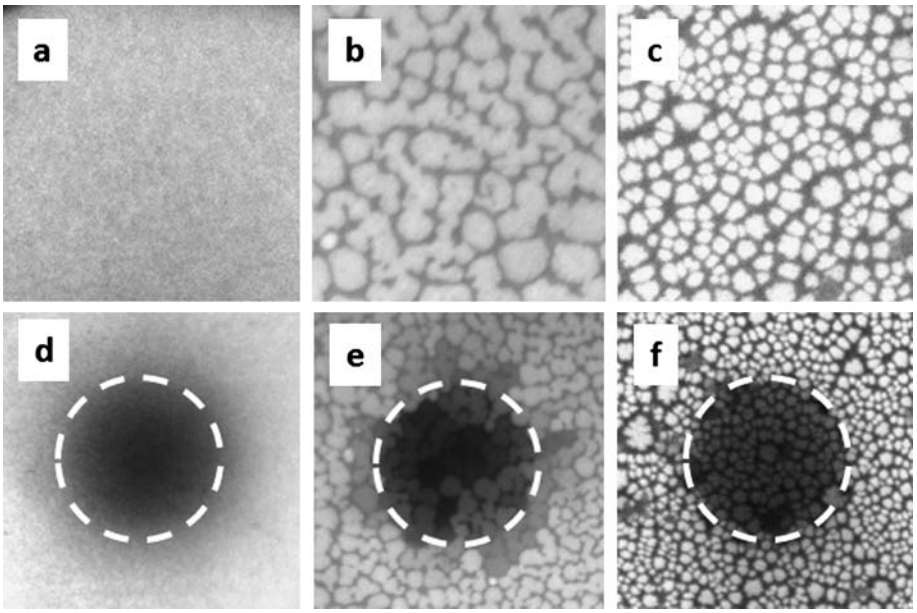


**Fig. 2** Epifluorescent micrographs (taken using 40× objective) of bilayers with 5 (a and d), 15 (b and e), and 30 (c and f) mol% DODA-$E_{85}$ in the LB layer, and SOPC in the LS layer, illustrating qualitatively the impact of lipopolymer concentration on membrane organization. The size for the top row is 50 μm × 50 μm; the size for the bottom row which also shows fluorescent recovery after photobleaching (FRAP) (2 min recovery after bleaching) is 100 μm × 100 μm. The dashed circle indicates the position and size of the bleaching spot.

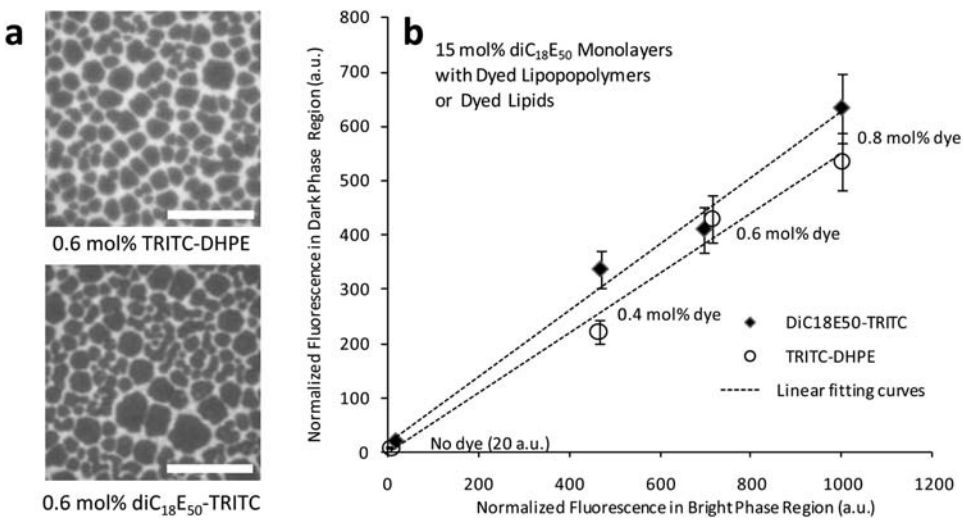


**Fig. 3** (a) EPI micrographs of LB monolayers with 15 mol% diC$_{18}$E$_{50}$, 84.4 mol% SOPC and 0.6 mol% either TRITC-DHPE (top) or diC$_{18}$E$_{50}$-TRITC (bottom). Scale bar is 10 μm. (b) Graph of relative fluorescence intensity in bright and dark regions for diC$_{18}$E$_{50}$-TRITC and TRITC-DHPE in LB monolayers with 15 mol% diC$_{18}$E$_{50}$. Data are taken from series of micrographs including those shown in (a), where fluorescence intensity is determined from relative grey values and normalized to arbitrary units (a.u.) where the bright region value for 0.8 mol% dye = 1000 a.u. Background values for the monolayer with no dye were also converted to a.u.

As expected, the phase patterns in Fig. 3a are quite similar to those of the DODA-$E_{85}$-containing bilayer system in Fig. 2, thus confirming the similarity of DODA-$E_{85}$ and diC$_{18}$E$_{50}$. Interestingly, there is a phase inversion between TRITC-DHPE-containing monolayer and bilayer micrographs in Fig. 2 and 3. In contrast, no phase inversion is observed if one compares the phase patterns of dye-labeled lipids and dye-labeled lipopolymers in Fig. 3a. This important result indicates that the existence of both phases cannot simply be attributed to lipid–lipopolymer phase separations in the LB monolayer. To confirm this qualitative finding, a quantitative analysis of the normalized fluorescence intensities of the dark and bright phases of comparable LB monolayers was conducted in the presence of 0.4, 0.6, and 0.8 mol% TRITC-DHPE and diC$_{18}$E$_{50}$-TRITC, respectively (Fig. 3b). This quantitative analysis showed that the fluorescence intensity in the dark phase is more than 16 fold higher than the background intensity (without dyes), thus excluding partial dewetting of the monolayer as a possible interpretation for the dark phase. Another notable result of Fig. 3b represents the linear relationship between changes in

normalized fluorescence intensities of dye lipids and dye lipopolymers in the bright and dark phases. The resulting slopes of the linear fitting curves in Fig. 3b suggest 1.6 and 1.8 fold enrichments of TRITC-DHPE and $diC_{18}E_{50}$-TRITC, respectively, in the bright phase. These almost identical enrichment values of both types of probe molecules confirm that dark and bright phases in Fig. 3a are not caused by phospholipid–lipopolymer demixing. Obviously, an alternative explanation must be sought to explain the existence of these two distinct phases. Therefore, we next explored the surface morphologies of a polymer-tethered SOPC monolayer and bilayer after LB and subsequent LB/LS transfers, respectively, using AFM. In both cases, the LB monolayer contains 30 mol% DODA-$E_{85}$. Fig. 4 illustrates representative height (a) and phase data (b) of the monolayer system, which are quite instructive. Fig. 4a demonstrates that the LB monolayer contains a series of connected ridges, such that the highest point on the monolayer extends about 2.5 nm from the base. The ridges have an average width of $\sim$1 μm, which is large in comparison to the length scale of individual lipopolymer molecules of 3–5 nm. The pattern similarity of ridge regions in Fig. 4a and bright phases in Fig. 3a provides a plausible explanation for the existence of two phases in the mixed lipopolymer–lipid LB monolayer at elevated lipopolymer molar concentration observed by EPI. In other words, non-planar regions (ridges) contain more lipid and lipopolymer material than planar (base) regions. The corresponding AFM phase mode image (Fig. 4b), which does not show a significant contrast between base and ridge regions, provides further evidence that the monolayer does not undergo a partial dewetting from the glass substrate, thus confirming the corresponding findings from EPI on LB monolayers presented in Fig. 3. These phase data also exclude partial lipopolymer crystallization as a possible reason for the formation of ridges in Fig. 4a. Such crystallization phenomena have been reported on crystallizable polymeric films.[41,42] The lack of lipopolymer crystallization in Fig. 4a is further supported by the observation that Langmuir monolayers of comparable poly(2-ethyl-2-oxazoline) lipopolymers maintain their fluidity at the LB transfer pressure of 30 mN $m^{-1}$.[43] Instead, the ridge and base regions in Fig. 4a can be interpreted in terms of a mechanism of buckle-driven delamination. Here the buckling/delamination can be explained in terms of the competing nature of attractive physisorption of lipopolymers on the solid substrate and repulsive forces between stretched polymer chains of neighboring lipopolymers. This competitive interaction behavior implies that lipopolymers in delaminated regions adopt entropically more favorable (less stretched) polymer conformations. Such a buckle-driven delamination process was recently also observed on polymer brushes, which were grown from an initiator and subsequently cross-linked to fabricate a film containing internal lateral compression stresses.[44] There, the partial delamination of the polymeric film was achieved by weakening thiol–gold polymer–substrate linkages using an electrical pulse. If the adsorption strength of polymer chains to the underlying solid is strong enough, polymers may also partially escape the lateral stress without desorption by stretching their chains.

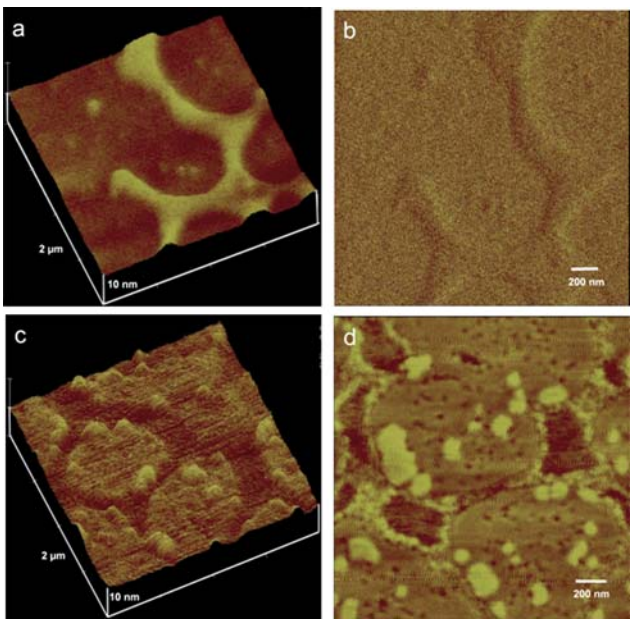


**Fig. 4** Height and phase images of LB monolayer and LB/LS bilayer with 30 mol% DODA-$E_{85}$ in LB layer, taken in air and in water, respectively. (a and b) The height and phase images for the monolayer system; (c and d) the film after subsequent LB and LS transfers. (Scale for phase images = 10°.)

Of even greater interest than the LB monolayer morphology is that of the bilayer constructed by subsequent LB and LS monolayer transfers. Fig. 4c and d illustrate corresponding height (c) and phase (d) data of such a bilayer system. Remarkably, a comparison of the LB data in Fig. 4a and b and the LB/LS data in Fig. 4c and d indicates that the ridge regions in the LB monolayer become valleys in the bilayer system with the average depth of the valleys being 2.0 ± 0.3 nm as found by inspection of a number of AFM micrographs of bilayers. Because such valley regions appear to act as lipid lateral diffusion barriers, we hypothesize that, unlike in base regions, no lipid bilayer can form over ridges of the LB monolayer.¶ Interestingly, the existence of butte-like morphologies near the rim of bilayer regions in Fig. 4c also suggests a dewetting-like process, which is often characterized by an accumulation of material into an advancing/retracting rim.[45] The corresponding phase image (Fig. 4d) shows that these butte-like regions are characterized by distinct viscoelastic properties. Previously, it has been reported that buckled, delaminated areas of a thin polymeric film may become nucleation sites for dewetting.[46]

To determine the underlying molecular process of bilayer compartmentalization in Fig. 2 and 4, we next modified the degree of hydrophilicity in the polymer moiety of lipopolymers. Unlike lipopolymers with highly hydrophilic polymers, those carrying moderately hydrophilic polymer chains (*e.g.*, DODA-$E_{85}$ and $diC_{18}E_{50}$) are more likely to escape the lateral stress imposed by polymeric crowding by penetrating through the hydrophobic lipid region of the LB monolayer. Consequently, the surfaces of delaminated ridge regions are expected to become

¶ At first glance, one might expect that since the ridges on the LB monolayer are roughly 2.5 nm higher than the rest of the substrate and the height of a lipid monolayer is about 2.5 nm, after LS-transfer the bilayer should have roughly the same height as the ridges of the monolayer after LB-transfer. However, this argument is not straightforward because the LB and LB/LS substrates represent different interfacial conditions.

less hydrophobic, which may eventually affect the ability of an LS monolayer to spread over such regions. To test the validity of these arguments, we conducted a set of EPI and AFM experiments on polymer-tethered monolayers and bilayers, in which the less hydrophilic poly(2-ethyl-2-oxazoline) lipopolymers were replaced by the more hydrophilic poly(2-methyl-2-oxazoline) lipopolymers ($diC_{18}M_{50}$). The enhanced hydrophilicity of poly(2-methyl-2-oxazoline) lipopolymers is exemplified by their lacking low-pressure transition in Langmuir monolayers that has been associated with adsorption/desorption of amphiphilic polymers at the air–water interface.[43,47] Fig. 5 shows FRAP/EPI data of model SOPC-$diC_{18}M_{50}$ bilayers after LB and LS transfers with 5 (a), 15 (b), and 30 mol% (c) $diC_{18}M_{50}$ in the bottom leaflet. Unlike corresponding DODA-$E_{85}$ containing polymer-tethered membranes (Fig. 2), no dark phases acting as lipid diffusion barriers are evident in any of the micrographs in Fig. 4, regardless of lipopolymer molar concentration.

To explore further the obvious differences between poly(2-ethyl-2-oxazoline) and poly(2-methyl-2-oxazoline) lipopolymer-containing polymer-tethered membranes in Fig. 2 and 5, the surface morphology of the latter systems was also investigated using AFM. Fig. 6 illustrates AFM height data of a polymer-tethered monolayer (left) and bilayer (right) containing 30 mol% $diC_{18}M_{50}$ in their LB monolayer. Instead of long ridges observed in the presence of DODA-$E_{85}$, the LB monolayer containing $diC_{18}M_{50}$ shows buckling into a series of small blisters, as illustrated in Fig. 6 (left). The scale in Fig. 6 is magnified 4× relative to the scale in Fig. 4 to better observe the smaller blisters. The height of the blisters is 4–5 nm above the lowest point. The existence of different buckling patterns in DODA-$E_{85}$- and $diC_{18}M_{50}$-containing membrane systems is not surprising, as theoretical models of compressed thin films elastically attached to rigid substrates predict a variety of buckling patterns found in real systems such as sputter deposited metal coatings.[48–50] These patterns include circular blisters, straight-sided blisters, and single and mesh-like undulating stripes. In all of these cases, their occurrence depends on multiple parameters, such as the applied lateral stress, the film elasticity, the film thickness, and the strength of adhesion between film and substrate. The more interesting result in Fig. 6 is that, unlike in the case of the DODA-$E_{85}$ system in Fig. 4, the surface morphology of the $diC_{18}M_{50}$-based bilayer system (Fig. 6 (right)) complements that of the corresponding monolayer (Fig. 6 (left)). This important finding indicates that the entire bilayer can be completed on top of a $diC_{18}M_{50}$-containing LB monolayer, regardless of the existence of blisters, thus explaining the good fluorescence recovery on $diC_{18}M_{50}$ containing membranes shown in Fig. 5.

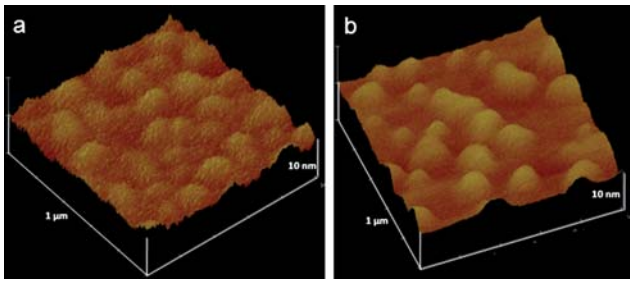


**Fig. 6** Height images of (a) LB monolayer (captured in air) and (b) LB/LS bilayer (captured under water) with 30 mol% $diC_{18}M_{50}$ in LB monolayer.

The different EPI, FRAP, and AFM results obtained from DODA-$E_{85}$- and $diC_{18}M_{50}$-based LB monolayers and LB/LS bilayers in Fig. 2–6 suggest different stress relaxation processes of lipopolymers associated with their distinct polymer hydrophilicities. Fig. 7 provides a proposed schematic of these distinct stress relaxation processes. In the case of the poly(2-ethyl-2-oxazoline)-containing lipopolymers DODA-$E_{85}$ and $diC_{18}E_{50}$, the amphiphilic nature of the ethyloxazoline moiety of the lipopolymers enables a stress relaxation process in which polymers detach from the solid substrate and partially penetrate into the hydrophobic lipid regions of the delaminated monolayer, thus making the surface of these regions more hydrophilic (Fig. 7a). As a result of such a polymer relaxation process, a lipid bilayer can only be formed outside of delaminated membrane regions (Fig. 7c). In the case of $diC_{18}M_{50}$, the higher hydrophilicity of the methyloxazoline polymer moiety prevents the penetration of polymer chains into the hydrophobic part of the monolayer in response to applied lateral stress (Fig. 7b). Because the surfaces of buckled regions retain their hydrophobicity, a bilayer can be formed on top of buckled and unbuckled regions (Fig. 7d). The above model highlights the importance of a subtle amphiphilic balance between lipid and polymer moieties of lipopolymers in the structure and dynamics of polymer-tethered lipid bilayer systems, as considered in this study. Interestingly, Szleifer and co-workers previously reported that the bilayer stability in lipopolymer-containing vesicles also depends on a subtle balance between the polymer chains and lipid tails and that stable lamellar bilayer structures can only be formed at relatively low lipopolymer concentrations of less than 10 mol%.[51] These

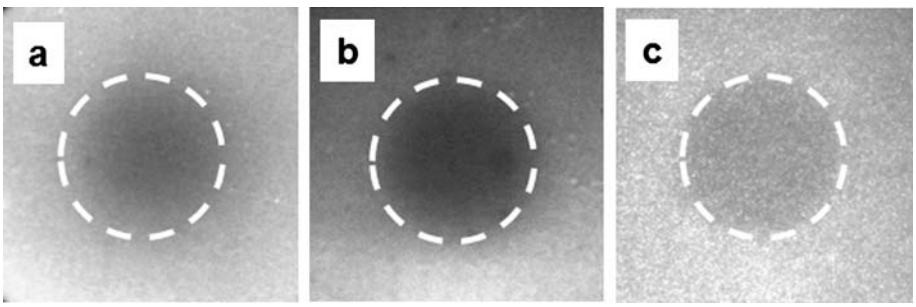


**Fig. 5** Epifluorescent micrographs (taken using 40× objective) showing FRAP of bilayers with 5 (a), 15 (b), and 30 (c) mol% $diC_{18}M_{50}$ in the LB layer, and SOPC in the LS layer. The size is 100 μm × 100 μm. The dashed circles indicate the position and size of the bleaching spot.

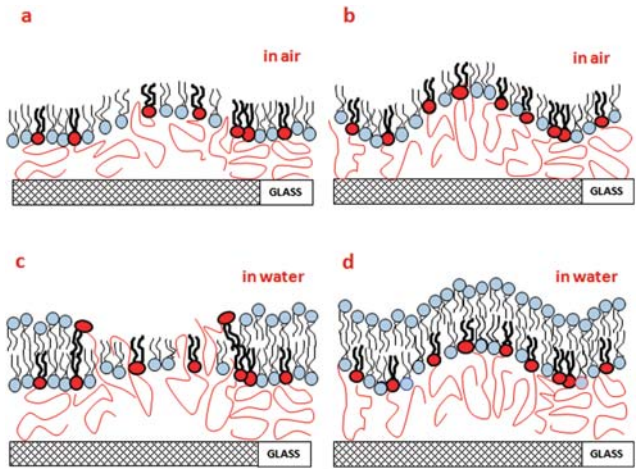


**Fig. 7** Schematic of stress relaxation processes in LB monolayers ((a) DODA-$E_{85}$, (b) di$C_{18}M_{50}$) and LB/LS bilayers ((c) DODA-$E_{85}$, (d) di$C_{18}M_{50}$), as derived from EPI, FRAP and AFM data, suggests the poly(2-ethyl-2-oxazoline) ($E_{85}$) moieties are more able to incorporate into the lipid monolayer than the poly(2-methyl-2-oxazoline) ($M_{50}$), disrupting the formation of a bilayer over the ridges for the DODA-$E_{85}$ bilayer, but not the di$C_{18}M_{50}$ bilayer. As described in the text, the extent of void formation under buckled regions partially depends on the strength of polymer adsorption to the glass substrate.

findings support the notion that planar polymer-tethered phospholipid bilayers at elevated lipopolymer concentrations, as studied in the current work, trigger the frustration of the entire membrane system, which is only counterbalanced by physisorption of polymer chains to the solid substrate. The prevention of the bilayer formation on top of delaminated membrane regions observed in the case of the DODA-$E_{85}$ system is intriguing because it can be seen as a process of buckling-induced dewetting of the LS monolayer.

Importantly, the observed process of buckling-induced dewetting of the LS monolayer in DODA-$E_{85}$-containing polymer-tethered lipid bilayers not only leads to a compartmentalization of the membrane, but also creates diffusion barriers between neighboring compartments. The EPI experiments in Fig. 2 imply that the compartment size and the permeability between compartments can be adjusted *via* the lipopolymer molar concentration, thus providing for the first time a lipid bilayer patterning approach where important properties can be tuned solely *via* lateral stress. To explore the impact of lipopolymer molar concentration on the permeability of diffusion boundaries between neighboring compartments, we next analyzed the lateral diffusion of QD-conjugated lipids in the top monolayer of DODA-$E_{85}$-containing polymer-tethered SOPC bilayers of various lipopolymer molar concentrations using SMFM. Unlike photo-labile dye-labeled lipids, these highly photostable QD-based tracking probes, which were recently developed in our laboratory,[35–37] allow long-time tracking experiments, thus probing μm size compartments found in this study. Fig. 8 illustrates representative $\langle r^2 \rangle$ *vs.* $\tau$ data from these QD lipid tracking experiments on polymer-tethered SOPC bilayers of 5, 15, and 30 mol% DODA-$E_{85}$, which allow a direct comparison to EPI experiments as illustrated in Fig. 2. Several important results can be obtained from these tracking data. Akin to diffusion studies carried out on live cells,[52] Fig. 8 shows that the tracking data are characterized by two different diffusion regimes described by the diffusion coefficients $D_{micro}$ and $D_{macro}$ and by a specific residency time, $\tau_{residency}$, associated with the time at the transition from $D_{micro}$ to $D_{macro}$. In plasma membranes, this diffusion behavior, also known as hop diffusion, is associated with the compartmentalization of the membrane into compartments of 30–230 nm diameter by the underlying cytoskeleton.[52–54] A comparison to the EPI fluorescence data in Fig. 2 suggests that the hop diffusion-like diffusion properties in ethyloxazoline-tethered phospholipid bilayers, illustrated in Fig. 7c, also reflect the compartmentalization of the bilayer, albeit into larger, μm size compartments. Inside bilayer compartments, the lipid diffusion is characterized by $D_{micro}$, whereas $D_{macro}$ describes length scales that exceed the average compartment size of the bilayer system. Interestingly, Fig. 8 also demonstrates that the difference between $D_{micro}$ and $D_{macro}$ becomes more pronounced with increasing lipopolymer molar concentration. This result indicates the ability to tune the permeability of the diffusion barriers *via* lipopolymer molar concentration in the current membrane system. The change in $D_{micro}$ with varying lipopolymer molar concentration implies that there are still substantial amounts of lipopolymers inside bilayer compartments, thus supporting previous single molecule tracking studies probing obstructed lipid/protein diffusion at a length scale of ~100 nm and agreeing with the results of Fig. 3.[14] Here it should be noted that the obstruction of QD tracking probes in the top monolayer by polymer-tethered lipids in the bottom monolayer is caused by a strong, transbilayer coupling of obstructed diffusion associated with a polymer-induced roughening of the bilayer, as recently reported by our group.[24] Interestingly, coupling of obstructed diffusion has also been observed in the presence of physisorbed polymers.[55] The average size of the

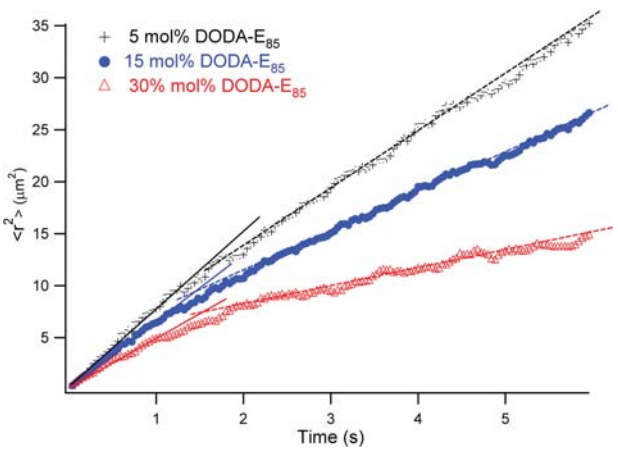


**Fig. 8** $\langle r^2 \rangle$ *vs.* $\tau$ plot of QD-conjugated lipid probes in fluid bilayers of 5, 15 and 30 mol% concentrations of DODA-$E_{85}$ in the LB layer, where solid lines indicate $4D_{micro}$, dashed lines indicate $4D_{macro}$, and $\tau_{residency}$ is the time at which the slope changes from $4D_{micro}$ to $4D_{macro}$. Each curve represents the average of 150 individual tracks of 150 steps each. The observed $D_{micro}$, $D_{macro}$ and $\tau_{residency}$ for the different polymer concentrations are as follows: 5 mol%, $D_{micro}$ = 2.08 μm$^2$ s$^{-1}$, $D_{macro}$ = 1.37 μm$^2$ s$^{-1}$, $\tau_{residency}$ = 0.90 s; 15 mol%, $D_{micro}$ = 1.63 μm$^2$ s$^{-1}$, $D_{macro}$ = 0.987 μm$^2$ s$^{-1}$, $\tau_{residency}$ = 1.13 s; 30 mol%, $D_{micro}$ = 0.958 μm$^2$ s$^{-1}$, $D_{macro}$ = 0.421 μm$^2$ s$^{-1}$, $\tau_{residency}$ = 1.83 s.

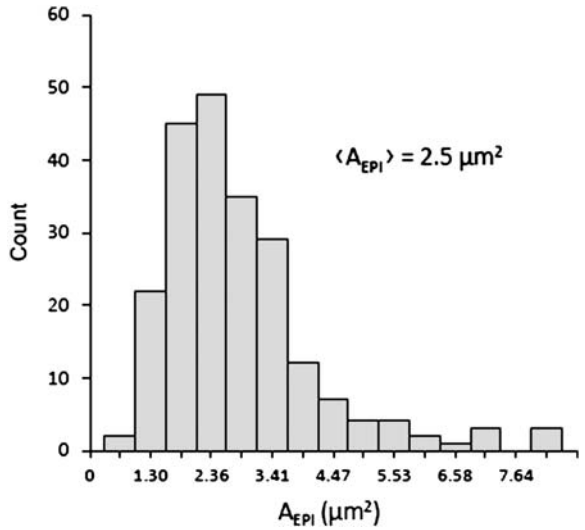


**Fig. 9** Histogram of 219 compartment areas ($A_{EPI}$) found from EPI images of a bilayer with 30 mol% DODA-E85 in the LB layer.

compartments $A_{SMFM}$ can be determined from $D_{macro}$ and $\tau_{residency}$ of the tracking data as previously described. Inspection of Fig. 2 suggests that eqn (1) is only appropriate for the closed or nearly closed compartments at 30 mol% DODA-$E_{85}$. In this case, $D_{macro}$ was determined from the slope of the $\langle r^2 \rangle$ *vs.* $\tau$ plot in Fig. 8 to be 0.42 $\mu m^2\ s^{-1}$ and $\tau_{residency}$ was found to be 1.83 s, which with eqn (1), leads to an average compartment size of $A_{SMFM} = 2.4\ \mu m^2$. Next we determined the average compartment size from the EPI micrographs of the polymer-tethered SOPC bilayer containing 30 mol% DODA-$E_{85}$, thus allowing a direct comparison to the corresponding compartment size obtained from single molecule tracking. Fig. 9 depicts a typical size histogram from such an EPI experiment. The histogram describing the size distribution of 219 individual compartments leads to the average compartment size of $A_{EPI} = 2.5 + 1.3\ \mu m^2$, which is in excellent agreement with the corresponding value found by the diffusion analysis. Unfortunately, we were unable to conduct similar tracking experiments on the di$C_{18}M_{50}$ containing membrane systems since the minimum time lag detectable by our SMFM system is insufficient to probe possible membrane heterogeneities associated with the submicron-sized buckling regions observed by AFM (Fig. 6). However, as described above, corresponding FRAP data of these systems suggest the formation of a continuous bilayer (see Fig. 5).

## Conclusion

In this work we have demonstrated that it is possible to compartmentalize bilayers by first applying lateral stress on a phospholipid monolayer through the addition of lipopolymers resulting in buckling and delamination, and next adding a second monolayer of pure lipids. Studies comparing poly(2-methyl-2-oxazoline) and poly(2-ethyl-2-oxazoline) lipopolymers indicate that bilayer compartmentalization is caused by penetration of polymeric chains of lipopolymers into the hydrophobic lipid regions of buckled, delaminated parts of the monolayer, thus preventing formation of the bilayer in those regions only. Most notably, unlike other existing lipid bilayer patterning approaches,[25–30] the patterning is achieved entirely by means of controlling the membrane composition and applying lateral stress. As our long-time single molecule tracking experiments using QD-conjugated lipids confirm, this novel feature provides, for example, a fascinating experimental tool to modify the permeability of diffusion barriers between bilayer compartments by simply adjusting lipopolymer molar concentration. In that sense, the described model membrane system is attractive to mimic length scale-dependent diffusion processes in cellular membranes. Even though this work has focused on lipopolymer-containing polymer-tethered lipid membranes, we envision that the basic concept of lateral stress regulation and buckling-induced dewetting can be applied to other polymer–lipid composite materials as well.

## Acknowledgements

This research was supported in part by the National Science Foundation (grant: MCB-0416779), the National Institute of Health (grant: R21 DK77051-01) and the IUPUI Nanoscale Imaging Center. Thanks also to Ricardo Decca, of the IUPUI Physics Department.

## Notes and references

1 J. G. A. Croll, *Int. J. Pavement Eng.*, 2008, **9**, 59–67.
2 R. C. Pangule, I. Banerjee and A. Sharma, *J. Chem. Phys.*, 2008, **128**, 234708.
3 K. Y. Lee, *Annu. Rev. Phys. Chem.*, 2008, **59**, 771–791.
4 L. Pocivavsek, R. Dellsy, A. Kern, S. Johnson, B. Lin, K. Y. Lee and E. Cerda, *Science*, 2008, **320**, 912–916.
5 M. K. Bera, M. K. Sanyal, S. Pal, J. Daillant, A. Datta, G. U. Kulkarni, D. Luzet and O. Konovalov, *Europhys. Lett.*, 2007, **78**, 56003.
6 C. Jiang, S. Singamaneni, E. Merrick and V. V. Tsukruk, *Nano Lett.*, 2006, **6**, 2254–2259.
7 P. J. Yoo, K. Y. Suh, S. Y. Park and H. H. Lee, *Adv. Mater.*, 2002, **14**, 1383–1387.
8 R. H. Notter and Z. Wang, in *Encyclopedia of Biomaterials and Biomedical Engineering*, ed. G. E. Wnek and G. L. Bowlin, Informa Healthcare, London, UK, 2004, vol. 2, p. 11.
9 D. Y. Takamoto, M. M. Lipp, A. von Nahmen, K. Y. C. Lee, A. J. Waring and J. A. Zasadzinski, *Biophys. J.*, 2001, **81**, 153–169.
10 S. Baoukina, L. Monticelli, M. Amrein and D. P. Tieleman, *Biophys. J.*, 2007, **93**, 3775–3782.
11 S. Baoukina, L. Monticelli, H. J. Risselada, S. J. Marrink and D. P. Tieleman, *Proc. Natl. Acad. Sci. U. S. A.*, 2008, **105**, 10803–10808.
12 E. Sackmann, *Science*, 1996, **271**, 43–48.
13 M. Tanaka and E. Sackmann, *Nature*, 2005, **437**, 656–663.
14 M. A. Deverall, E. Gindl, E. K. Sinner, H. Besir, J. Rühe, M. J. Saxton and C. A. Naumann, *Biophys. J.*, 2005, **88**, 1875–1886.
15 M. L. Wagner and L. K. Tamm, *Biophys. J.*, 2000, **79**, 1400–1414.
16 M. L. Wagner and L. K. Tamm, *Biophys. J.*, 2001, **81**, 266–275.
17 O. Purrucker, A. Förtig, R. Jordan and M. Tanaka, *ChemPhysChem*, 2004, **5**, 327–335.
18 O. Purrucker, S. Gonnenwein, A. Förtig, R. Jordan, M. Rusp, M. Barmann, L. Moroder, E. Sackmann and M. Tanaka, *Soft Matter*, 2007, **3**, 333–336.
19 R. Robelek, E. Lemker, B. Wiltschi, V. Kirste, R. Naumann, D. Oesterhelt and E.-K. Sinner, *Angew. Chem., Int. Ed.*, 2007, **46**, 605–608.
20 O. Purrucker, A. Förtig, R. Jordan, E. Sackmann and M. Tanaka, *Phys. Rev. Lett.*, 2007, **98**, 078102.
21 S. Garg, J. Rühe, K. Lüdtke, R. Jordan and C. A. Naumann, *Biophys. J.*, 2007, **92**, 1263–1270.
22 V. Kiessling, J. M. Crane and L. K. Tamm, *Biophys. J.*, 2006, **91**, 3313–3326.

23 P. C. Seitz, M. D. Reif, O. V. Konovalov and R. Jordan, *ChemPhysChem*, 2009, **10**, 2876–2883.
24 M. A. Deverall, S. Garg, K. Lüdtke, R. Jordan, J. Rühe and C. A. Naumann, *Soft Matter*, 2008, **4**, 1899–1908.
25 J. Groves, N. Ulman and S. Boxer, *Science*, 1997, **275**, 651–653.
26 C. K. Yee, M. L. Amweg and A. N. Parikh, *Adv. Mater.*, 2004, **16**, 1184–1189.
27 A. M. Smith, T. Huser and A. N. Parikh, *J. Am. Chem. Soc.*, 2007, **129**, 2422–2423.
28 K. Morigaki, H. Schönherr and T. Okazaki, *Langmuir*, 2007, **23**, 12254–12260.
29 J. Shi, J. Chen and P. Cremer, *J. Am. Chem. Soc.*, 2008, **130**, 2718–2719.
30 T. Okazaki, T. Inaba, Y. Tatsu, R. Tero, T. Urisu and K. Morigaki, *Langmuir*, 2009, **25**, 345–351.
31 K. Ritchie, X. Y. Shan, J. Kondo, K. Iwasawa, T. Fujiwara and A. Kusumi, *Biophys. J.*, 2005, **88**, 2266–2277.
32 J. T. Lehman, PhD thesis, Gutenberg-Universitat Mainz, Germany, 1999.
33 K. Lüdtke, R. Jordan, P. Hommes, O. Nuyken and C. A. Naumann, *Macromol. Biosci.*, 2005, **5**, 384–393; R. Jordan, K. Martin, H. J. Räder and K. K. Unger, *Macromolecules*, 2001, **34**, 8858–8865.
34 R. Jordan, K. Graf, H. Riegler and K. K. Unger, *Chem. Commun.*, 1996, 1025–1026.
35 M. J. Murcia, D. Shaw, H. Woodruff, C. A. Naumann, B. Young and E. Long, *Chem. Mater.*, 2006, **18**, 2219–2225.
36 M. J. Murcia, D. Shaw, E. Long and C. A. Naumann, *Opt. Commun.*, 2008, **281**, 1771–1780.
37 M. J. Murcia, D. E. Minner, G. M. Mustata, K. Ritchie and C. A. Naumann, *J. Am. Chem. Soc.*, 2008, **130**, 15054–15062.
38 C. A. Naumann, O. Prucker, T. Lehmann, J. Rühe, W. Knoll and C. W. Frank, *Biomacromolecules*, 2002, **3**, 27–35.
39 S. L. Frey, D. Zhang, M. A. Carignano, I. Szleifer and K. Y. C. Lee, *J. Chem. Phys.*, 2007, **127**, 114904.
40 O. Purrucker, A. Förtig, K. Lüdtke, R. Jordan and M. Tanaka, *J. Am. Chem. Soc.*, 2005, **127**, 1258–1264.
41 H. G. Braun and E. Meyer, *J. Phys.: Conf. Ser.*, 2008, **126**, 012027.
42 G. Reiter, G. Castelein and J.-U. Sommer, *Macromol. Symp.*, 2002, **183**, 173–178.
43 C. A. Naumann, C. F. Brooks, G. G. Fuller, T. Lehmann, J. Rühe, W. Knoll, P. Kuhn, O. Nuyken and C. W. Frank, *Langmuir*, 2001, **17**, 2801–2806.
44 S. Edmondson, K. Frieda, J. E. Comrie, P. R. Onck and W. T. S. Huck, *Adv. Mater.*, 2006, **18**, 724–728.
45 I. Karapanagiotis, W. W. Gerberich and D. F. Evans, *Langmuir*, 2001, **17**, 2375–2379.
46 T. G. Stange, D. F. Evans and W. A. Hendrickson, *Langmuir*, 1997, **13**, 4459–4465.
47 K. Lüdtke, R. Jordan, N. Furr, S. Garg, K. Forsythe and C. A. Naumann, *Langmuir*, 2008, **24**, 5580–5584.
48 G. Parry, A. Cimetiere, C. Coupeau, J. Colin and J. Grilhe, *Phys. Rev. E: Stat. Phys., Plasmas, Fluids, Relat. Interdiscip. Top.*, 2006, **74**, 066601–066607.
49 E. A. Jagla, *Phys. Rev. B: Condens. Matter*, 2007, **75**, 085405–085408.
50 A. Volinsky, *Mater. Res. Soc. Symp. Proc.*, 2004, **795**, 816–886.
51 M. Rovira-Bru, D. H. Thompson and I. Szleifer, *Biophys. J.*, 2002, **83**, 2419–2439.
52 T. Fujiwara, K. Ritchie, H. Murakoshi, K. Jacobson and A. Kusumi, *J. Cell Biol.*, 2002, **157**, 1071–1081.
53 K. Murase, T. Fujiwara, Y. Umemura, K. Suzuki, R. Iino, H. Yamashita, M. Saito, H. Murakoshi, K. Ritchie and A. Kusumi, *Biophys. J.*, 2004, **86**, 40754093.
54 K. Suzuki, K. Ritchie, E. Kajikawa, T. Fujiwara and A. Kusumi, *Biophys. J.*, 2005, **88**, 3659–3680.
55 L. Zhang and S. Granick, *Macromolecules*, 2007, **40**, 1366–1368.


 